New events discovered in the Apollo lunar seismic data

R. C. Bulow, C. L. Johnson,[1] and P. M. Shearer

Cecil H. and Ida M. Green Institute of Geophysics and Planetary Physics, Scripps Institution of Oceanography, University of California, San Diego, La Jolla, California, USA

Received 8 February 2005; revised 11 July 2005; accepted 15 July 2005; published 27 October 2005.

[1] We use modern seismological data processing tools to revisit the Apollo lunar seismic data set with the goal of extending and further characterizing the existing catalog of deep moonquakes. Our studies focus on the long-period data and include filtering and despiking noisy data, event classification, cluster identification, and robust methods for amplitude estimation. We perform cross-correlation analyses for known groups of deep events, confirming earlier visual classifications. By combining the cross-correlation approach with a robust median despiking algorithm, we produce improved differential times and amplitudes, enabling us to construct cleaner stacks. Each event group, represented by a single waveform stack of its constituent members, is cross correlated with the continuous time series. We focus on the A1 cluster because it has more cataloged events than any other cluster and is generally well characterized. Using this approach, we identify additional events that can be associated with previously defined deep clusters. For the deep event group A1 we have found 123 new events, which show phase behavior similar to the 323 previously cataloged events. Our new event search allows us to create optimized event stacks with improved signal to noise from which revised travel time picks (and thus location estimates) can be made. Application of our methods to other deep clusters should form a more complete event catalog and improve our understanding of the spatial and temporal distribution of deep lunar events.

Citation: Bulow, R. C., C. L. Johnson, and P. M. Shearer (2005), New events discovered in the Apollo lunar seismic data, *J. Geophys. Res.*, *110*, E10003, doi:10.1029/2005JE002414.

1. Introduction

[2] The Apollo Passive Seismic Experiment (PSE) consisted of four seismometers placed on the lunar surface between 1969 and 1972 as part of the Apollo Lunar Surface Experiment Package. The seismometers were deployed by astronauts on the Apollo 11, 12, 14, 15, and 16 missions. Each station included three long-period instruments (one vertical and two horizontal components, sample rate 6.625 Hz) and one short-period instrument (vertical component, sample rate 53.00 Hz). Continuous data from stations 12, 14, 15, and 16 (the Apollo 11 instrument failed after one lunar day) were telemetered to Earth and recorded until 1977.

[3] Analysts visually inspected the records in order to identify seismic events. Early studies classified events into four main types: artificial impacts (such as the booster rockets ejected from the command module), natural impacts (meteoroids), shallow moonquakes occurring at depths of 50–220 km [*Khan et al.*, 2000; *Lognonné et al.*, 2003], and deep moonquakes (natural events with focal depths between 700 and 1000 km). Events were classified using a variety of criteria, including waveform matching, risetime, spectral characteristics, shear wave identification, and time of occurrence [*Lammlein et al.*, 1974]. Over 12,000 events have been identified, more than half of which (6549) are deep moonquakes [*Nakamura et al.*, 2004]. Most studies performed on the lunar seismic data have concentrated on these previously identified events, which contain data starting 10 min before the detected signal onset and lasting until that signal attenuates below the noise level, often an hour or more later.

[4] Early analyses of the lunar event data included the generation of seismic velocity models with different types of events used to infer information about different regions in the lunar interior. For example, because artificial impacts create seismic events of known location and origin time at relatively small distances from the stations (median distance 172 km), energy recorded from these impacts provides information on crustal structure: thickness and seismic velocities to approximately 100 km depth [e.g., *Toksöz et al.*, 1972, 1974]. In contrast, accurately locating meteroid impacts and moonquakes is challenging because of the small number of stations, the poor signal-to-noise ratio of many of the records, the often emergent *P* wave arrivals, and the strong *P* wave coda that hampers identification of *S* wave arrivals. Nonetheless, subsets of these events have

[1] Also at Department of Earth and Ocean Sciences, University of British Columbia, Vancouver, British Columbia, Canada.

0148-0227/05/2005JE002414

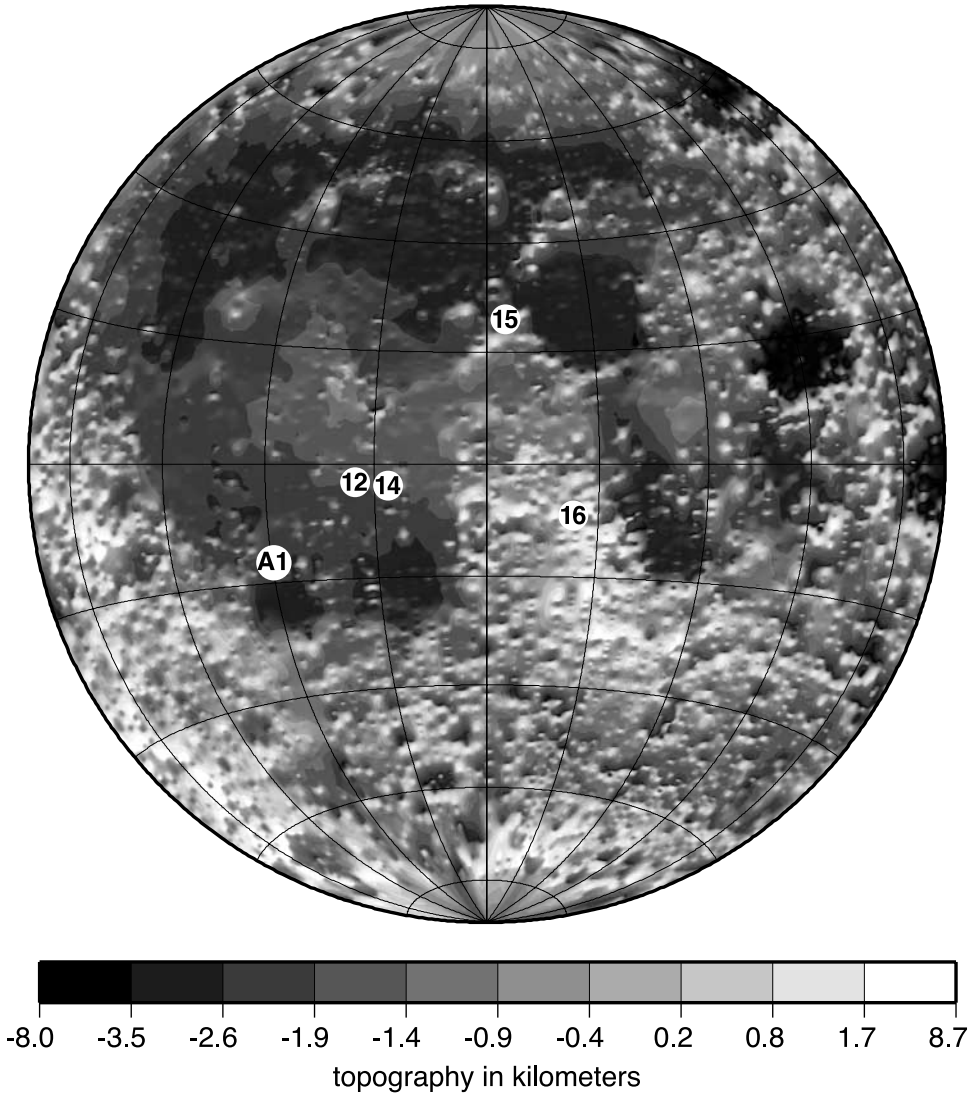

Figure 1. Topographic map [*Zuber et al.*, 1994] of the nearside of the moon showing station locations and the epicenter of the A1 deep event group.

been used to estimate lunar seismic velocity profiles down to about 1000 km, the depth of the deepest moonquakes [*Nakamura et al.*, 1976; *Dainty et al.*, 1976; *Goins et al.*, 1981; *Nakamura et al.*, 1982; *Nakamura*, 1983; *Khan et al.*, 2000; *Lognonné et al.*, 2003]. Seismic velocity structure at depths greater than 1000 km is not known because of the lack of deeper events and definitively identified far side events.

[5] Deep moonquakes are the most numerous type of event recorded by the PSE. These events appear to originate from specific source regions, each of which produces repeatable waveforms [*Lammlein*, 1977]. Early classifications were made by visual inspection and matching of waveforms. Seismograms printed on translucent paper were compared by placing one atop another on an illuminated table. The most current event catalog still lists events selected from the continuous data in this manner. A combination of waveform cross correlation and single-link cluster analysis performed on this catalog [*Nakamura*, 2003] has identified clusters of associated deep events from more than 300 distinct source regions. However, as the cataloged events were originally detected by eye, it is possible that many low signal-to-noise events may have been overlooked. Modern computing capabilities provide motivation to analyze the continuous data. Waveform correlations can be performed systematically, enabling the quantification of similarities among deep moonquakes and the objective detection of such events in the continuous time series.

[6] Two characteristics of deep moonquakes are especially notable: seismograms from each deep event source region are highly repeatable, and correlate in time with lunar tides [*Lammlein et al.*, 1974]. The waveform repeatability allows us to use stacking and cross-correlation methods to search for previously undetected events in the continuous data. Newly identified events can be added to the existing catalog [*Nakamura et al.*, 2004]. The application of cross-correlation techniques to all events in our expanded catalog enables robust identification of events associated with a specific deep cluster, including our new events, and previously unclassified or incorrectly classified events. This can yield event stacks with increased signal to noise and better

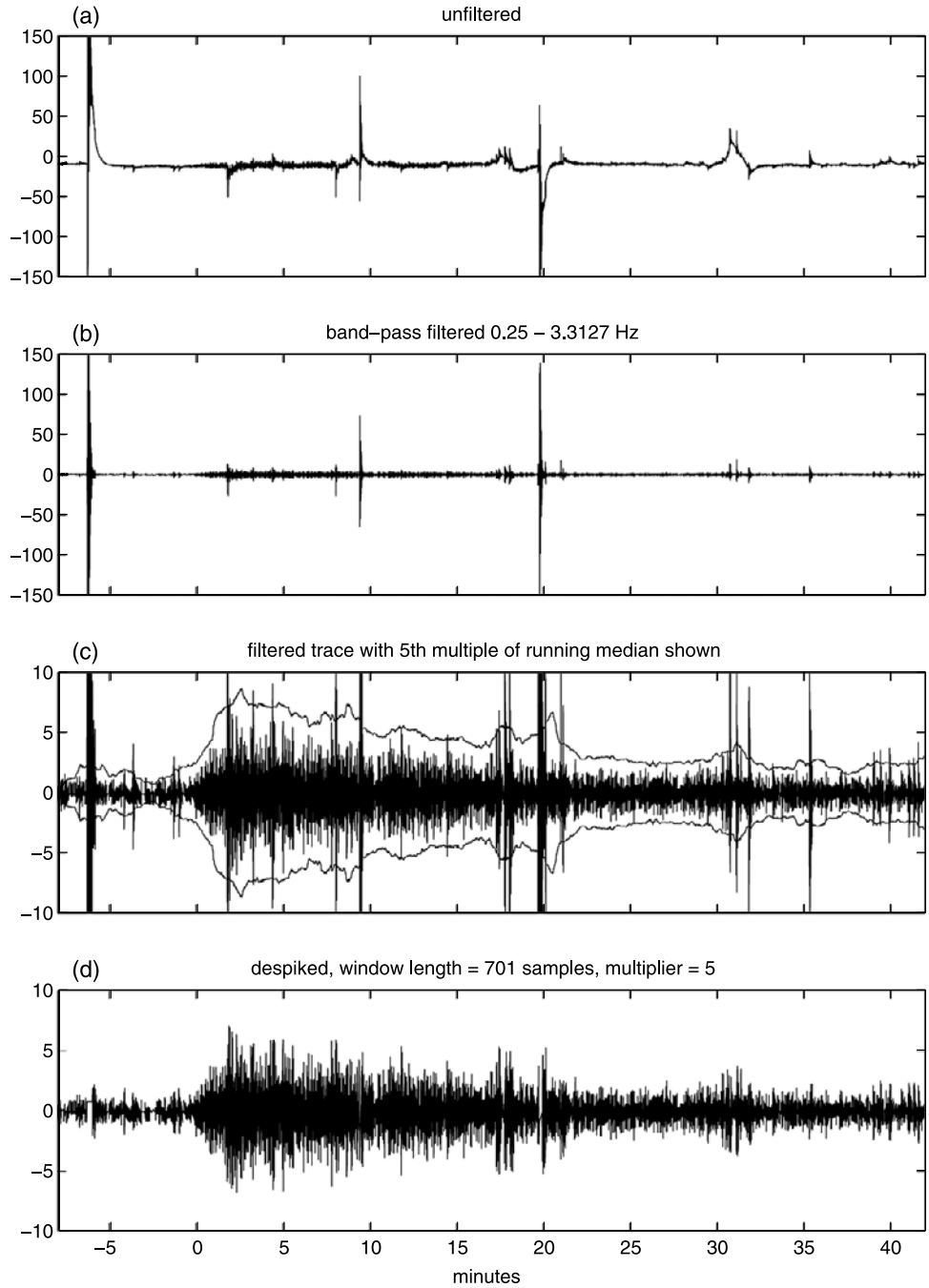

Figure 2. Benefits of filtering and despiking. (a) Unfiltered A1 trace from deep event occurring on 1977/149 at 1136 UT. The record shown is component lpx at station 14. Note that the dynamic range in the record is dominated by high-amplitude thermal spikes such as those near −7, 2, 10, and 20 min. (b) Same trace after application of band-pass filter (0.25–3.3127 Hz). (c) Same trace with 5 times the running median value outlined. (d) Same trace after application of running median despiker (window length 701 samples and median multiplier 5).

seismic phase identification, from which we can pick travel times and estimate cluster hypocenters.

[7] Previous studies have suggested that the periodicity of deep moonquake occurrence times results from the buildup and release of tidal stresses [*Lammlein et al.*, 1974; *Lammlein*, 1977; *Toksöz et al.*, 1977]. This further motivates our interest in obtaining a more complete catalog of deep moonquakes, as improved temporal information for each event cluster will allow for more accurate analyses of tidal periodicities.

[8] In this paper, we demonstrate how the existing lunar deep event database can be improved through the analysis of the A1 cluster (Figure 1). We focus on A1 as it is the cluster with the most cataloged events (323 as identified by *Nakamura et al.* [2004]) and has been the subject of many previous studies [e.g., *Lammlein et al.*, 1974; *Lammlein*,

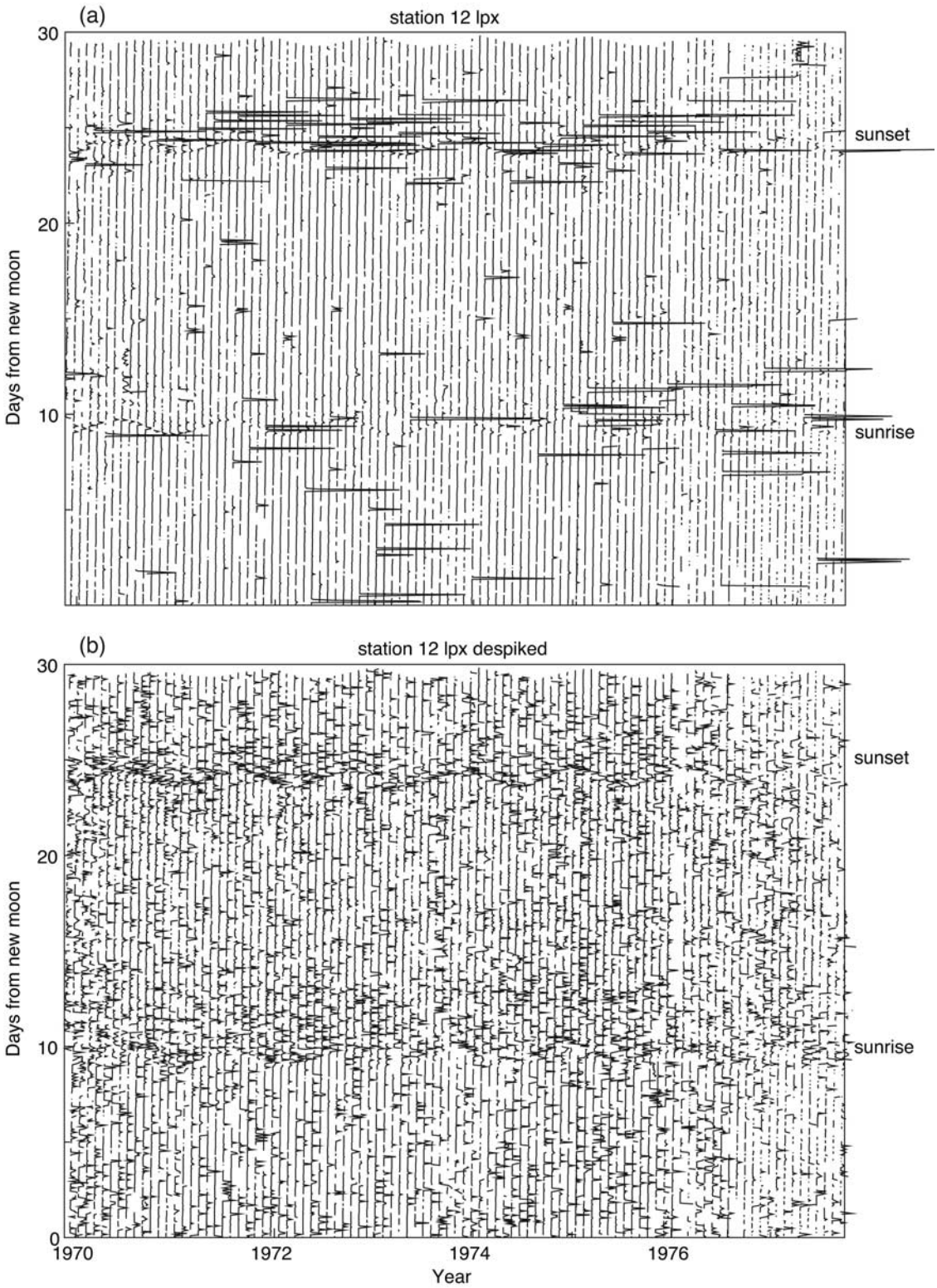

Figure 3. (a) Continuous data synodic phase versus occurrence time for station 12. The maximum peak-to-peak amplitude in 1-hour time intervals determines the magnitude of the horizontal deviations from the slightly angled continuous lines defined by the synodic phase (days) versus the absolute time (years). Sunrise and sunset times are noted. The maximum amplitudes exhibit a sinusoidal behavior consistent with the varying length of the lunar synodic month. (b) Same plots after despiking the data. Note daytime noise has been greatly reduced. In this case, amplitudes are enlarged by a factor of 10 compared to Figure 3a.

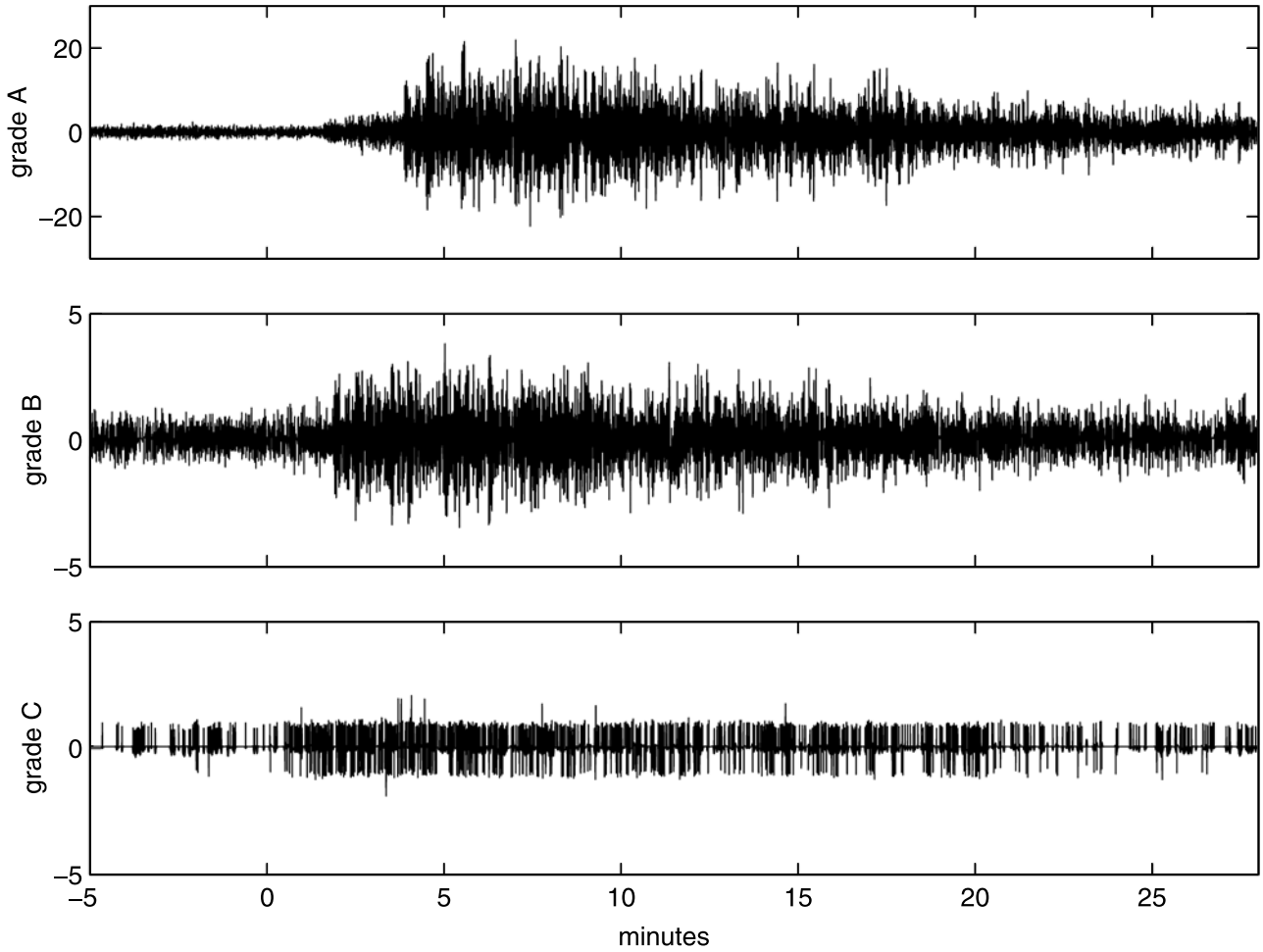

Figure 4. Examples of assigned grades for three events from the A1 cluster. Grade A shows event at station 16 lpy component occurring on 1975/304 at 0634 UT. Grade B shows event at station 16 lpy component occurring on 1975/333 on 0815 UT. Grade C shows event at station 12 lpx component occurring on 1970/189 at 1809 UT.

1977; *Nakamura*, 1978; *Toksöz et al.*, 1977]. However, our approach is general and can be extended to other deep clusters. We document the techniques and data processing steps required in some detail since our analysis begins with the lunar seismic data in its original format. Although much of this information is available in previous papers and technical reports, our analyses have been greatly helped by additional information provided through personal communication with investigators who originally worked with the PSE data. We hope that the synthesis provided here will prove useful to those wishing to use this challenging data set in the future.

[9] We first describe initial processing steps applied to both the event and continuous time series to remove potentially erroneous records, filter, and despike the seismograms (section 2). We conduct a qualitative assessment of the seismograms for previously cataloged events: a visual inspection of records to provide familiarity with the data set and to obtain an estimate of the percentages of data that are of a specified quality.

[10] Our new event search has so far focused on the A1 cluster. We begin with the preparation of a *target trace* for cross correlation: a representative A1 event stack used to identify all potential A1 events from the continuous data (section 3). We perform cross correlations between the stack and the continuous data, noting the times of peaks in the correlation function for comparison to cataloged event times. Correlation peak occurrence times not coinciding with cataloged event times [*Nakamura et al.*, 2004] may represent new events. New event records are distinguished from noise by requiring the absolute value of the cross-correlation function to be greater than a threshold value (section 4). We validate these new events (section 5) by stacking them to enhance their signal levels and by comparing their occurrence times to tidal periodicities recognized previously for the A1 cluster [*Lammlein et al.*, 1974; *Toksöz et al.*, 1977; *Lammlein*, 1977]. The methods used to discover new events can also be applied to identify all events associated uniquely with A1 and to optimize event stacks. These stacks produce improved signal-to-noise records for measuring *P* and *S* arrival times. Our methodology should be applicable to other deep event clusters, where the discovery of additional events will assist in location and tidal periodicity

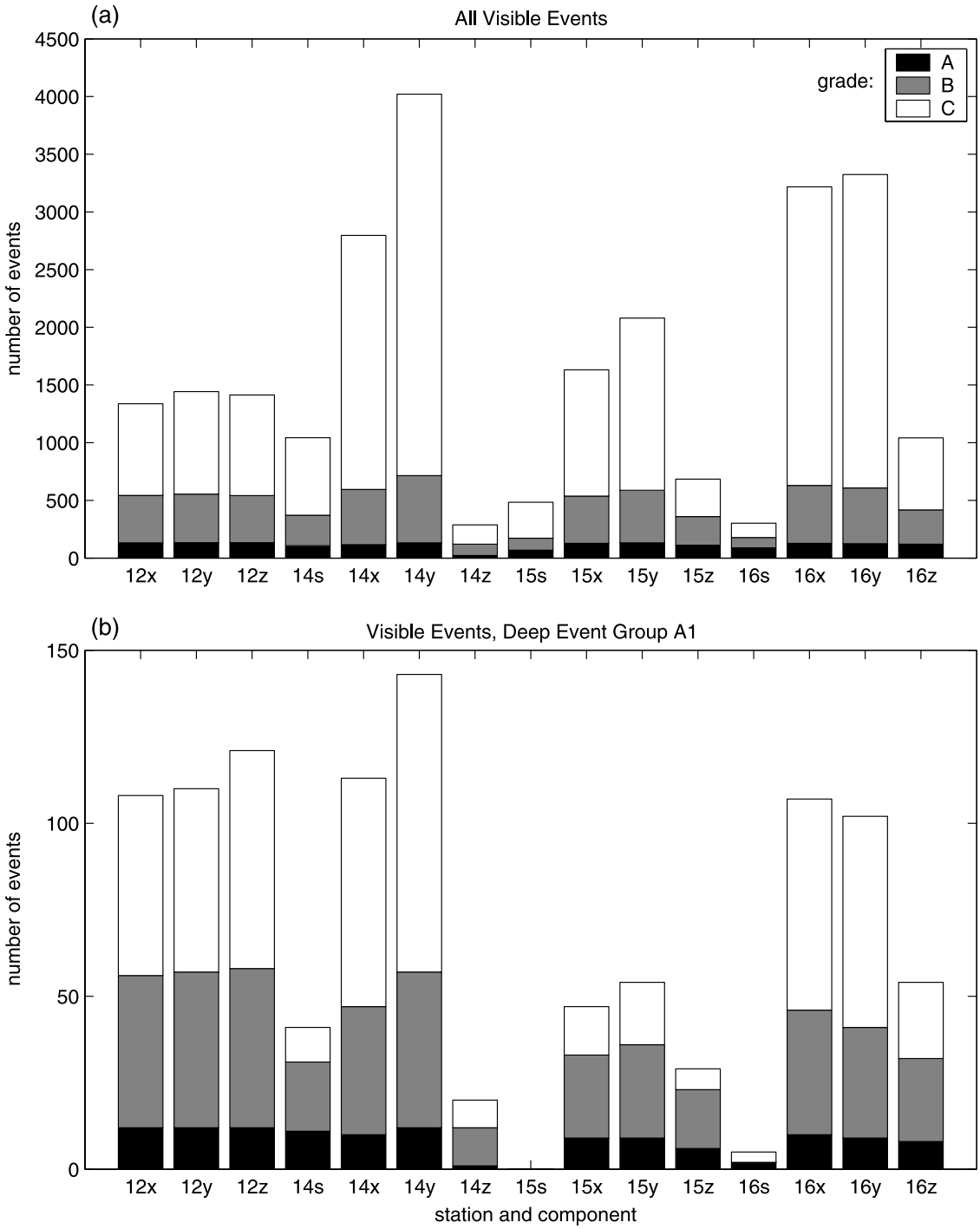

Figure 5. Histograms of visible events per station and component for (a) all events and (b) deep event group A1. The station 12 short-period component is not shown as that channel was inoperative for a majority of the experiment.

studies, particularly for the smaller, less well-identified clusters.

2. Data Preparation

[11] The lunar seismic data are currently available from the IRIS Data Management Center (www.iris.edu) either via exabyte tape request or by ftp. Both event data and continuous data are available. The event tapes contain events reported in the catalog of *Nakamura et al.* [2004]. The continuous data tapes are available as two separate groups: the PSE (Passive Seismic Experiment) tapes archiving the seismic data up until 1976 Julian day 60, and the Normal Bit-Rate Work tapes which archive the

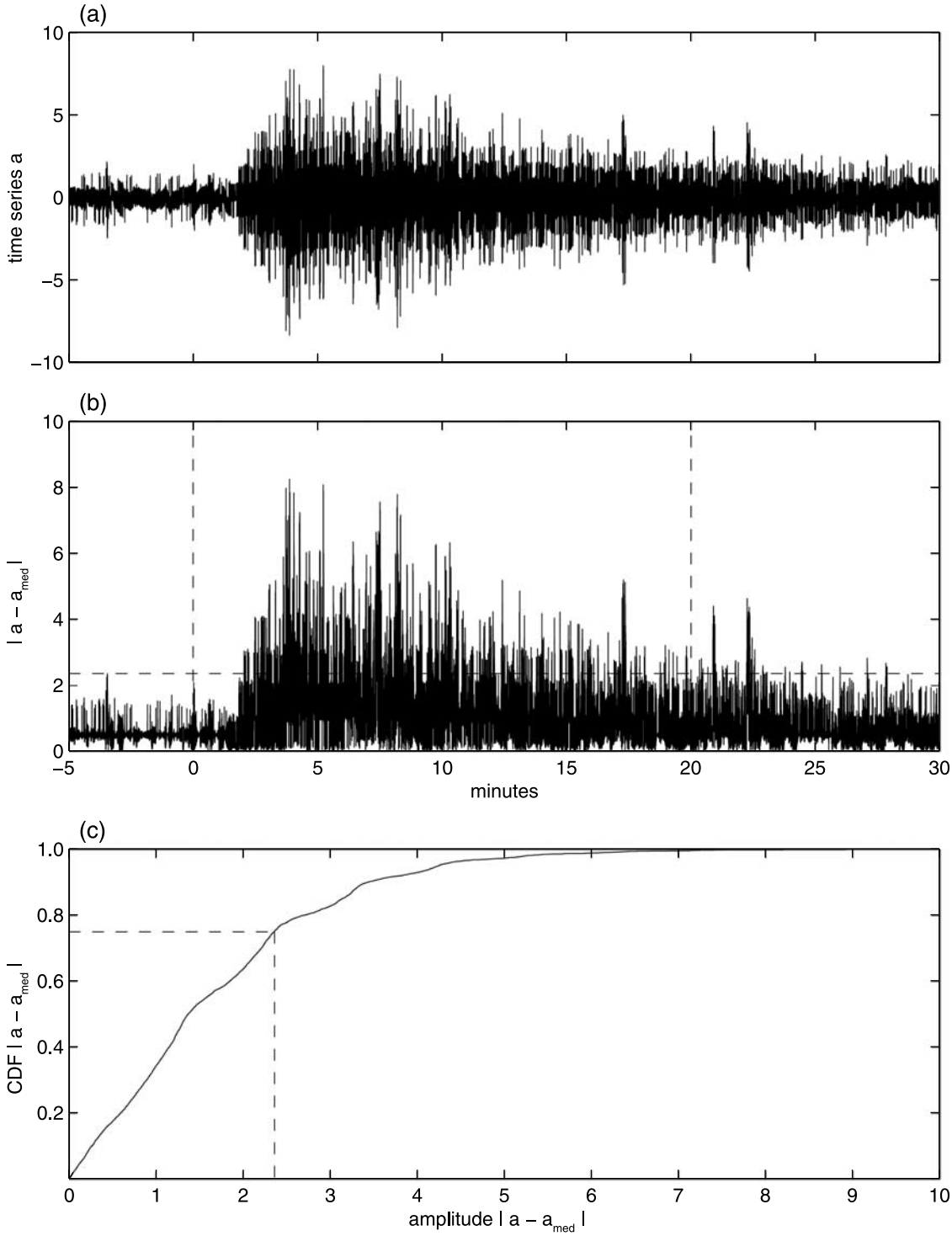

Figure 6. Example of our amplitude estimation method. (a) Time series *a*, an event occurring at station 14 lpx component on 1971/187 at 1652 UT. (b) Absolute deviation of time series about the median value (a_{med}). (c) Cumulative distribution function of $|a - a_{med}|$. Dashed line shows location of 75th percentile. In Figure 6b vertical dashed lines show time window used in Figure 6c, and horizontal dashed line shows amplitude as determined in Figure 6c.

data from that time until the end of the experiment on Julian day 273, 1977. These two types of continuous lunar seismic data have minor differences in format; both are available from IRIS.

[12] Each tape consists of a series of records. Read errors from the original magnetic tapes occasionally resulted in the fragmentation of a record. Other problems were introduced by instrument sensitivity to temperature fluctuations

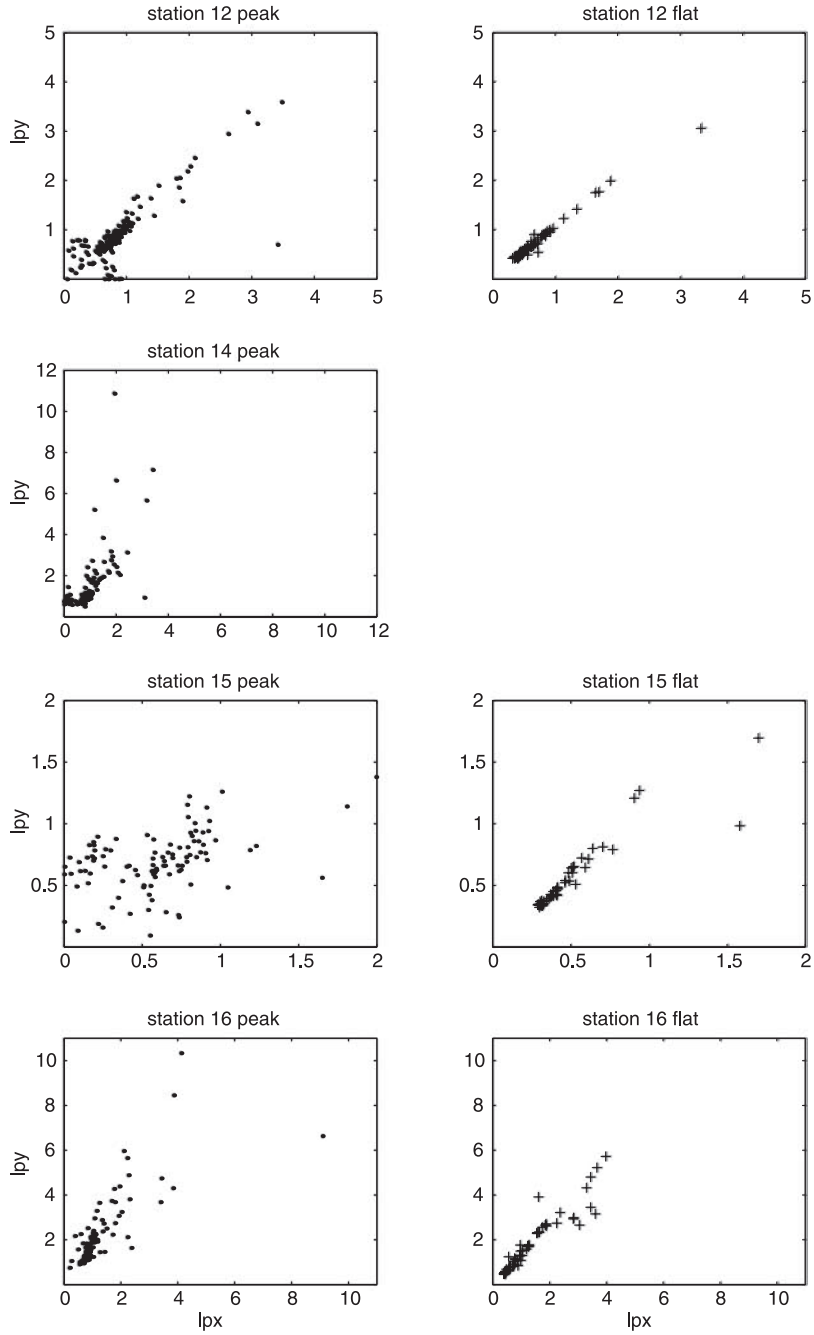

Figure 7. Amplitudes of all A1 events per station, *x* component versus *y* component. Crosses (circles) indicate events during time when stations were operated in "flat" ("peak") mode (note station 14 only operated in peak mode). Amplitudes generally agree with the expected 1:1 correlation on the horizontal channels. For the flat mode events the scatter is greatly reduced.

between lunar day and night, telemetry errors, and the limited dynamic range of the instruments (10 bit sampling). In general, the quality of lunar seismograms is low compared to typical terrestrial seismograms. In addition, strong scattering and low attenuation result in emergent arrivals and extended codas for both *P* and *S* waves.

[13] Each long-period instrument could be operated in one of two modes: "peak" or "flat" (broader band) response [*Lammlein et al.*, 1974]. Operating the instruments in flat mode sometimes made them unstable, so for the most part the stations were operated in peak mode. This latter mode had a higher gain, which was fortunate owing to the low dynamic range of the instruments and the small magnitude of natural seismic signals. Additionally, the resonant period of the instruments in peak mode is 2.2 s, coincident with the frequency range of deep moonquakes. Nonetheless, from Julian day 180, 1975 (1975/180), to day 86, 1977 (1977/086), stations 12, 15, and 16 were operated in "flat" mode, in which the instrument response was extended to lower frequencies. (Station 12 was also operated in the flat

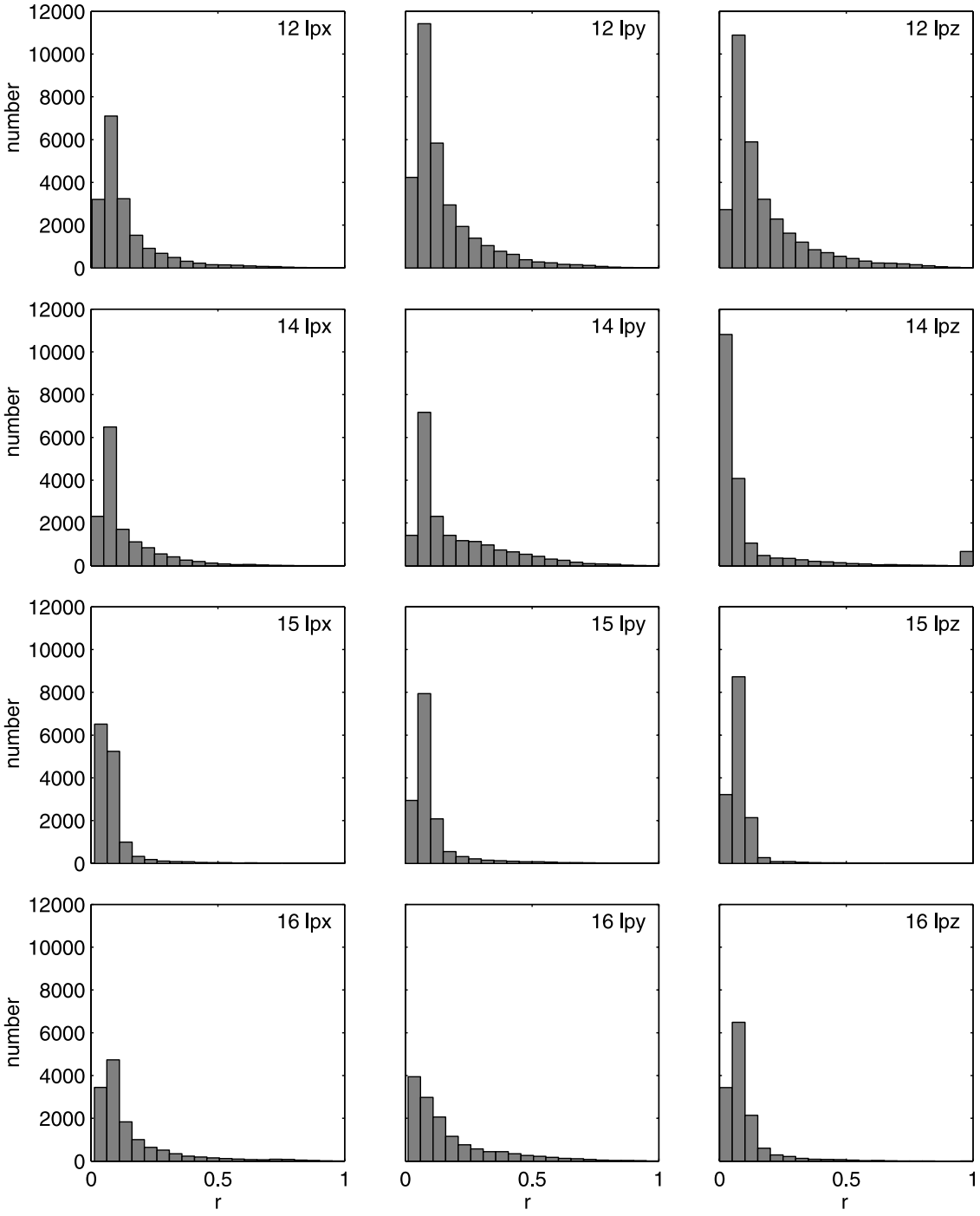

Figure 8. Histograms of correlation coefficient values for deep event group A1 (323 events). Correlations are performed station by station and component by component.

mode from 1974/289 to 1975/99.) In this mode, the long-period seismometers have a level response from 1 to 15 s [*Lammlein et al.*, 1974].

[14] The analog seismometer output was digitized and telemetered directly to Earth. Various digitization irregularities were common as the digitization of seismic traces was still in its infancy when the lunar data were gathered. Error checks and filtering performed on the event and continuous data are described below. Our processing began with the conversion of files from their original format to a format used in analyses of terrestrial seismic data and adapted for the lunar data. During this conversion procedure we conducted the following checks:

[15] 1. The software time flag check indicates that one of the receiving stations had difficulty reading the standard time signal, and a computer-generated time was substituted. Such times may be off by as much as several seconds from the standard time.

[16] 2. The sync pattern check compares a bit string in the data to the Barker code and its complement. Barker codes

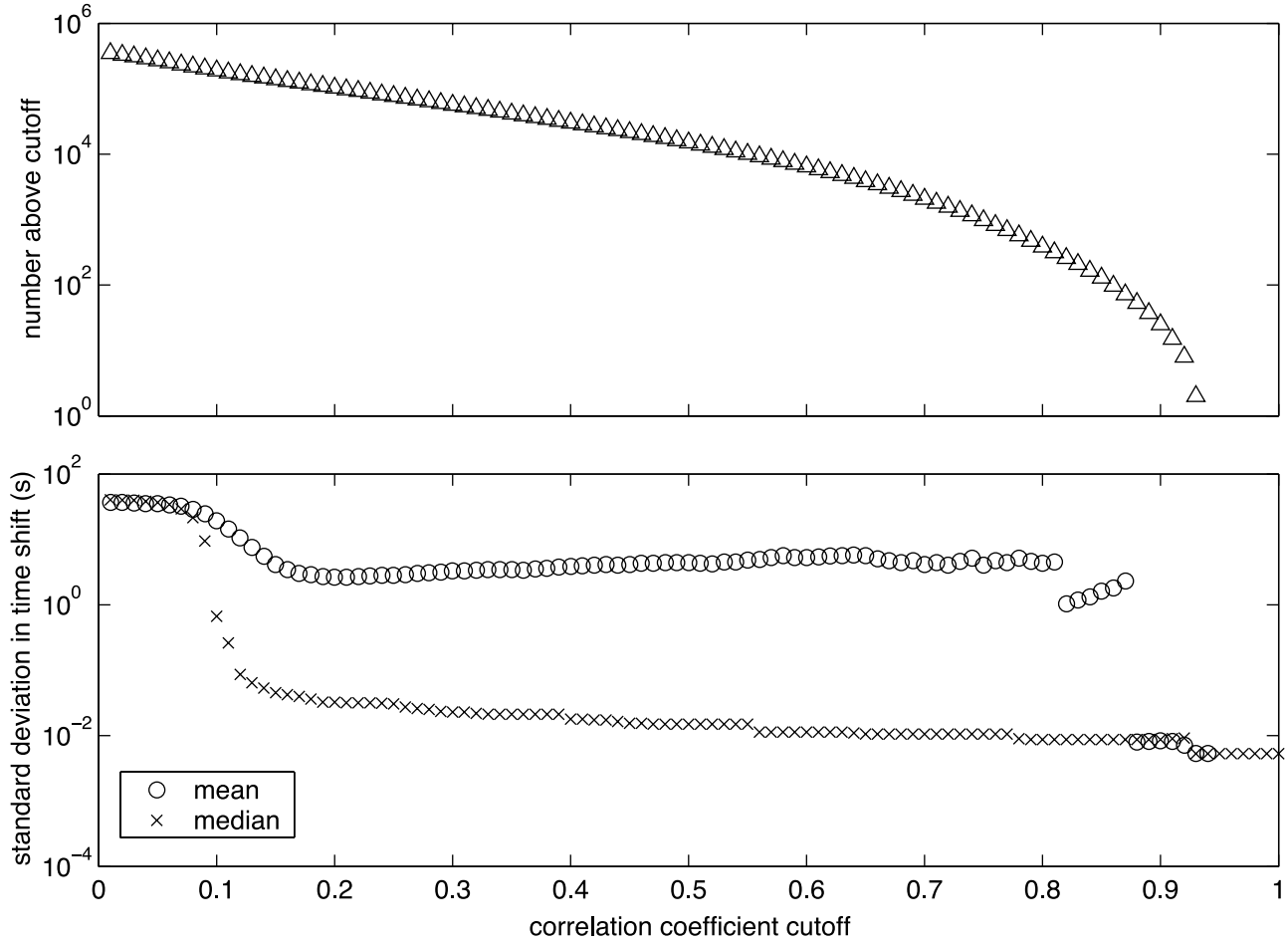

Figure 9. Mean (circles) and median (crosses) standard deviation in time shifts (seconds) versus correlation coefficient cutoff for correlations performed between members of the deep event group A1 (peak mode). Also shown is the total number of event pairs falling above the cutoff (triangles). The discontinuities in the mean value occur when anomalously high standard deviations are dropped as the cutoff is raised.

are commonly used for frame synchronization in digital communication systems. If the bit string in the data does not match the code, the data are out of sync.

[17] 3. The timing mismatch check is computed as $(t_c - t_p) - \Delta t$ where t_c and t_p are the times of the current and previous records, respectively, and Δt is the predicted time difference assuming evenly sampled data. We considered records more than 0.5 s off from the previous record unusable.

[18] In this study, we discard records containing any of the above errors since the precise time correction required for reliable timing information is unknown. To remove long-period fluctuations and secular trends from the data, we band-pass filter the traces from 0.25 Hz to the Nyquist frequency (3.3127 Hz). However, some large-amplitude anomalies characterized by sharp onsets and exponential amplitude decay pass through the filter and emerge as spikes (Figures 2a and 2b). These spikes are observed on all stations and are most intense near lunar sunrise and sunset; they are likely caused by the thermal expansion and contraction of the insulating shroud protecting each instrument [*Lammlein et al.*, 1974].

Table 1. Number of Catalogued A1 Events Stacked

		Number of A1 in Target Stack		Available A1 Stacked	
Station	Channel	Peak	Flat	Peak,[a] %	Flat,[b] %
12	lpx	139	51	61.8	60.7
	lpy	154	55	68.4	65.5
	lpz	63	59	28.0	70.2
14	lpx	144	-	61.3	-
	lpy	165	-	70.2	-
	lpz	19	-	8.1	-
15	lpx	26	13	17.0	17.8
	lpy	40	24	26.1	32.9
	lpz	9	15	5.9	20.6
16	lpx	75	48	63.0	57.1
	lpy	70	51	58.8	60.7
	lpz	46	26	38.7	31.0

[a]Values given are out of 225, 235, 153, and 119 A1 events for stations 12, 14, 15, and 16, respectively.
[b]Values given are out of 84, 73, and 84 A1 events for stations 12, 15, and 16, respectively.

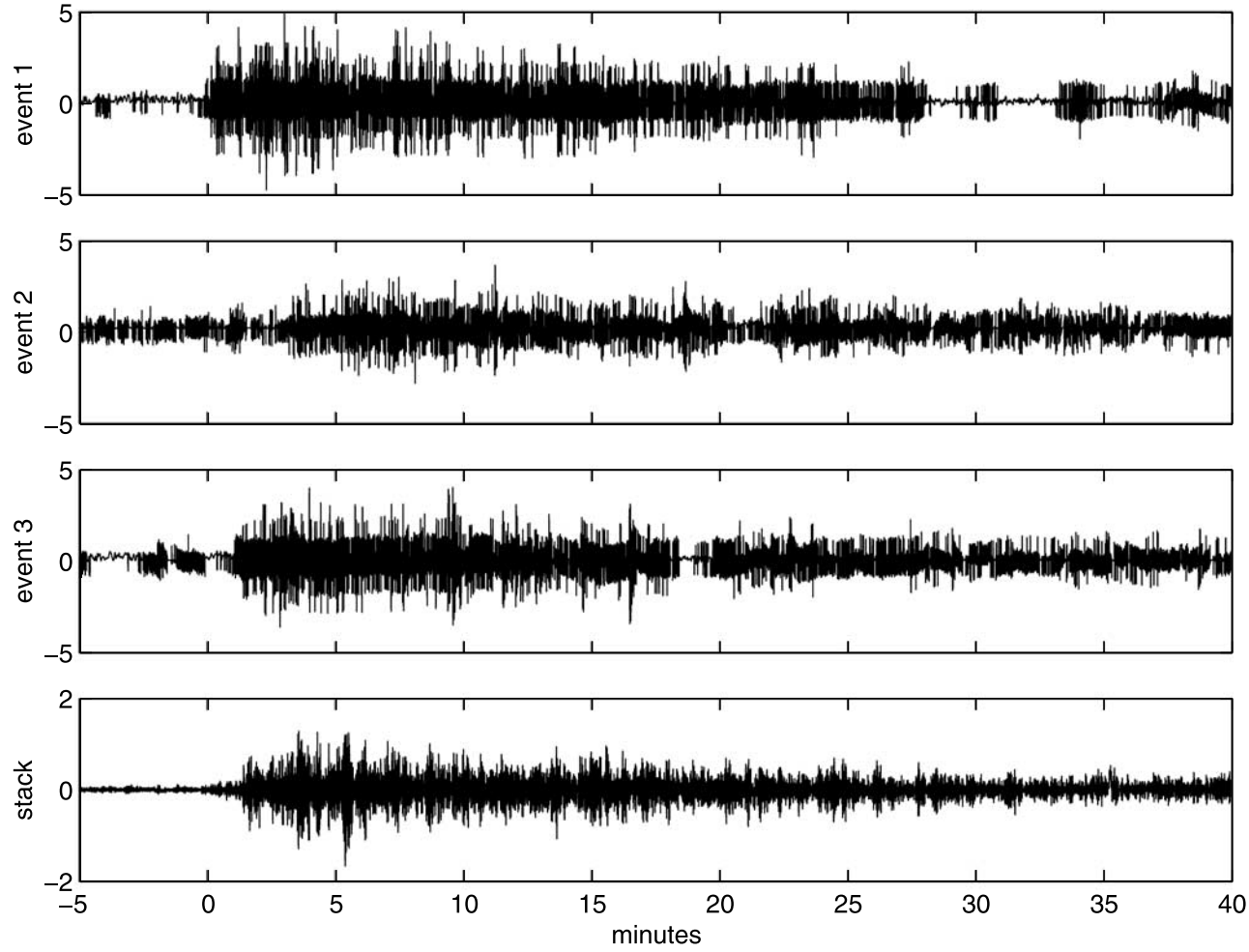

Figure 10. A1 stack and representative traces (all are station 12, lpx component). Event 1 occurred on 1970/009 at 0203 UT. Event 2 occurred on 1971/080 at 1628 UT. Event 3 occurred on 1973/201 at 1902 UT.

[19] The association of noise spikes with lunar sunrise and sunset is illustrated in Figure 3, in which we show the maximum peak-to-peak amplitudes in 1-hour time windows as a function of time since the last new moon (the phase relative to the 29.53-day period of the synodic month, or the time between two consecutive new moons) for continuous data from station 12. The noisiest parts of the records occur near the times of lunar sunrise and sunset, and in general the records are noisier during the daytime. Figure 3 also illustrates gaps in the data as recovered from the tape archives; these gaps amount to only about 1% of the total time period.

[20] We remove noise spikes and thermal anomalies from our filtered records using a robust median despiking algorithm [*Evans*, 1982] to avoid bias in event amplitude estimation and other calculations. We compute the median value of the time series in a running window of length m samples. Points within the window that lie above a user-specified multiple of the median are removed and replaced with a linear interpolation of the data across the spikes. A trace that has been despiked using a window length of 701 samples (approximately 2 min) and a median multiplier of 5 is shown in Figures 2c and 2d. Experimentation showed that these parameter values result in a relatively conservative despiking method that removes the largest anomalies associated with the spikes with minimal clipping of actual data. Despiking also improves phase/time plots, emphasizing the correlation between noise spikes and lunar sunrise and sunset (Figure 3b).

3. Analysis of Previously Identified Deep Moonquakes

[21] To familiarize ourselves with the lunar data, we analyze previously detected deep moonquakes for which event seismograms are available. We visually inspect this entire data set to evaluate event quality and distribution. Next, we assess A1, the largest of the deep clusters, examining event amplitudes and correlations among waveforms. The results are used to establish selection criteria for A1 events that can be stacked to create target traces. These traces are then used to find previously undetected events in the continuous time series.

3.1. Qualitative Event Characteristics: All Events

[22] We apply a manual "grading" technique in which all cataloged events [*Nakamura et al.*, 2004] are inspected

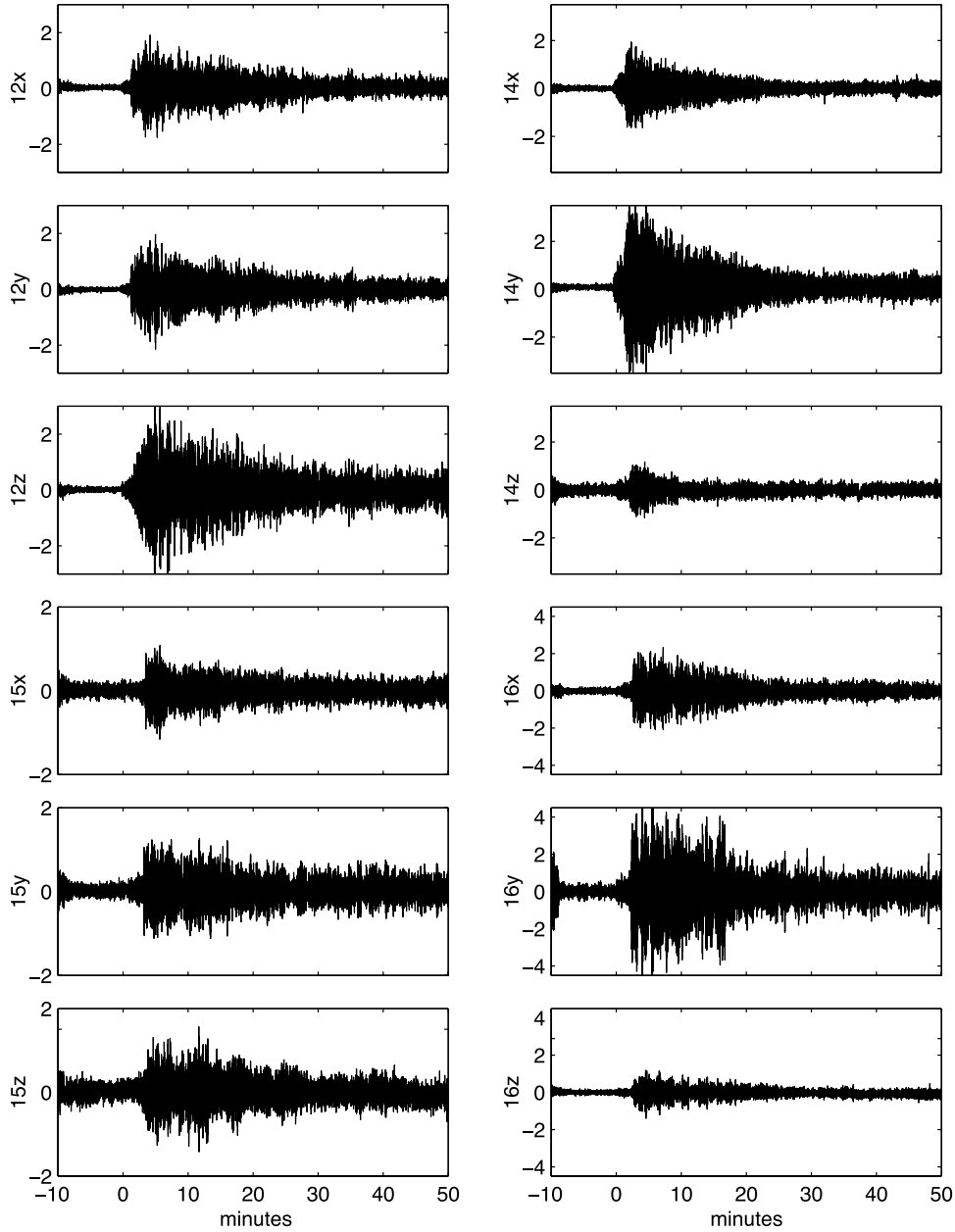

Figure 11. A1 peak mode stacks. For each station all long-period components are plotted on the same scale to show amplitude variability. Note differences in scaling among stations.

visually and assigned a grade of A, B, or C based on the quality of their traces. In the grading process we consider several factors, including signal to noise, initial impulse coherence, the shape of the envelope function, and the appearance of the event on one or more of the long-period channels. This grading allows for easy selection of subsets of high-, medium-, or low-quality traces for later analyses (Figure 4).

[23] A trace receiving the grade "A" generally has high signal to noise and an impulsive onset, and seismic phases may be visible. A grade "B" trace has somewhat lower signal to noise and a more gradual emergence, but a distinct envelope is still evident. A grade "C" trace has inferior signal to noise and the entire event trace is often dominated by amplitudes of a single digital unit, with the event seen as a region in the trace with a greater frequency of 1-bit fluctuations between high and low. While events may (optimistically) be detected from such traces, any estimation of event amplitude or timing is problematic. The percentages of events receiving grades A, B, and C are 2%, 8%, and 57% respectively, with 33% remaining ungraded (i.e., of poorer quality than grade "C"), representing 263, 1019, 7127, and 4149 of the 12,558 events in the *Nakamura et al.* [2004] catalog.

[24] We consider a previously cataloged event "visible" if it received a grade during this process. Events not receiving a grade were not readily distinguishable from background noise (and in fact were originally detected only after processing with an unconventional filter). Significant variability in the total number of "visible" events is seen

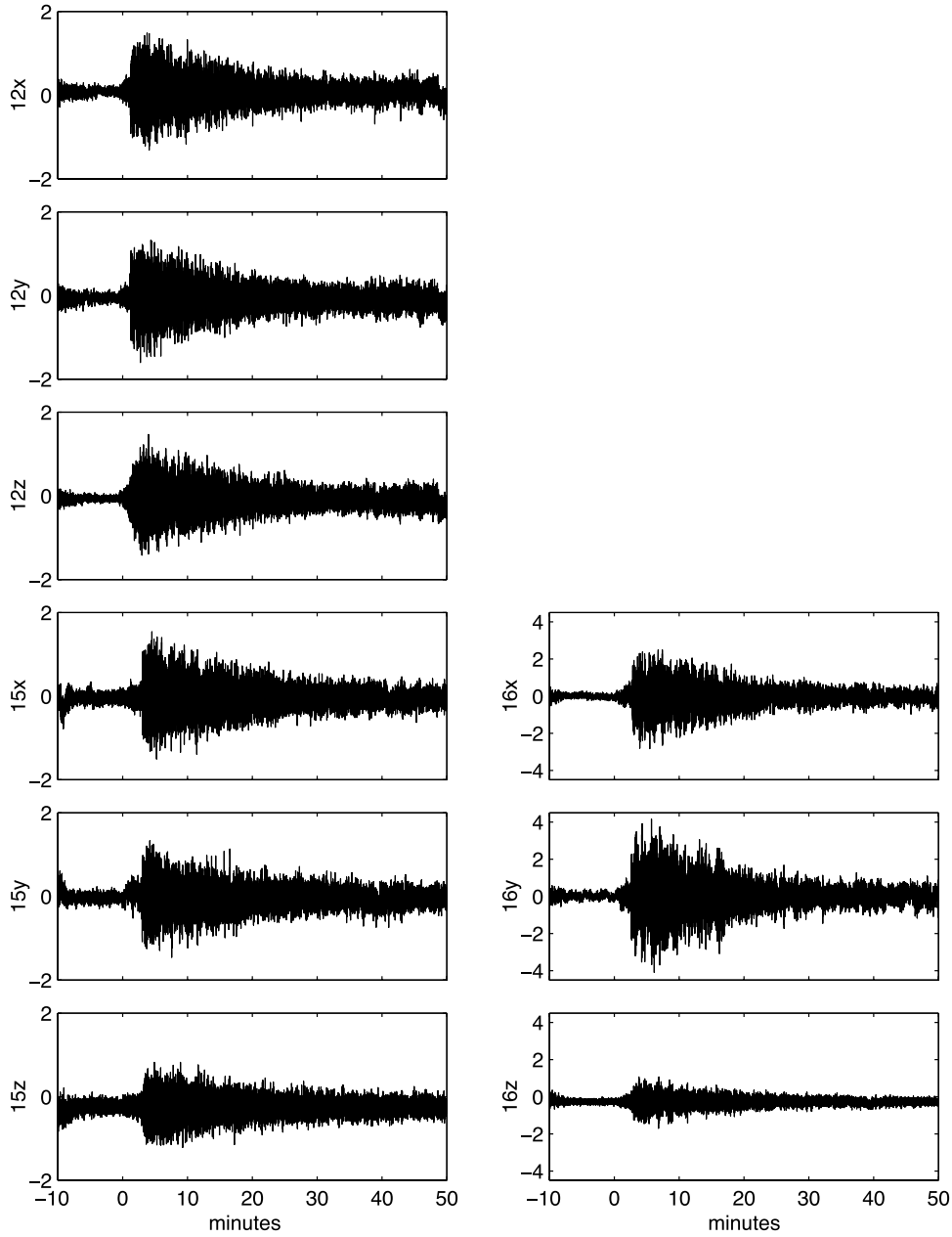

Figure 12. A1 flat mode stacks (with the exception of station 14, which was not operated in flat mode).

among different stations and for a given station among the *x*, *y*, and *z* channels. Histograms of event visibility by station and channel are shown in Figure 5a for all events and Figure 5b for the deep event group A1 alone.

[25] Similar patterns in the relative number of visible events are seen for all events and for the A1 group. However, the A1 cluster has higher relative visibility on station 12 compared to stations 14 and 16 (Figure 5b) than that of all events (Figure 5a). This is likely due to the proximity of the A1 source to station 12 (Figure 1). Two additional station characteristics are apparent in Figure 5. First note that the long-period *z* component of station 14 was inoperative for most of the deployment and did not record many seismograms. Second, the A1 events (and deep moonquakes in general) tend not to appear in the short-period seismograms. (Note that there is no data for the station 12 short-period instrument, which failed shortly after deployment.) Because of this, we restrict our analyses of deep events to the long-period data.

3.2. Quantitative Event Characteristics: Deep Cluster A1

[26] The deep event cluster A1 has the most cataloged events and is the focus of further quantitative studies, including amplitude estimation and waveform cross correlation.

3.2.1. Event Amplitude Estimation

[27] We investigated several methods for estimating event amplitudes in order to identify a consistent amplitude measure despite the poor signal-to-noise ratio exhibited by a majority of the traces. These included relative amplitudes calculated through cross correlation and several different estimates of absolute amplitude.

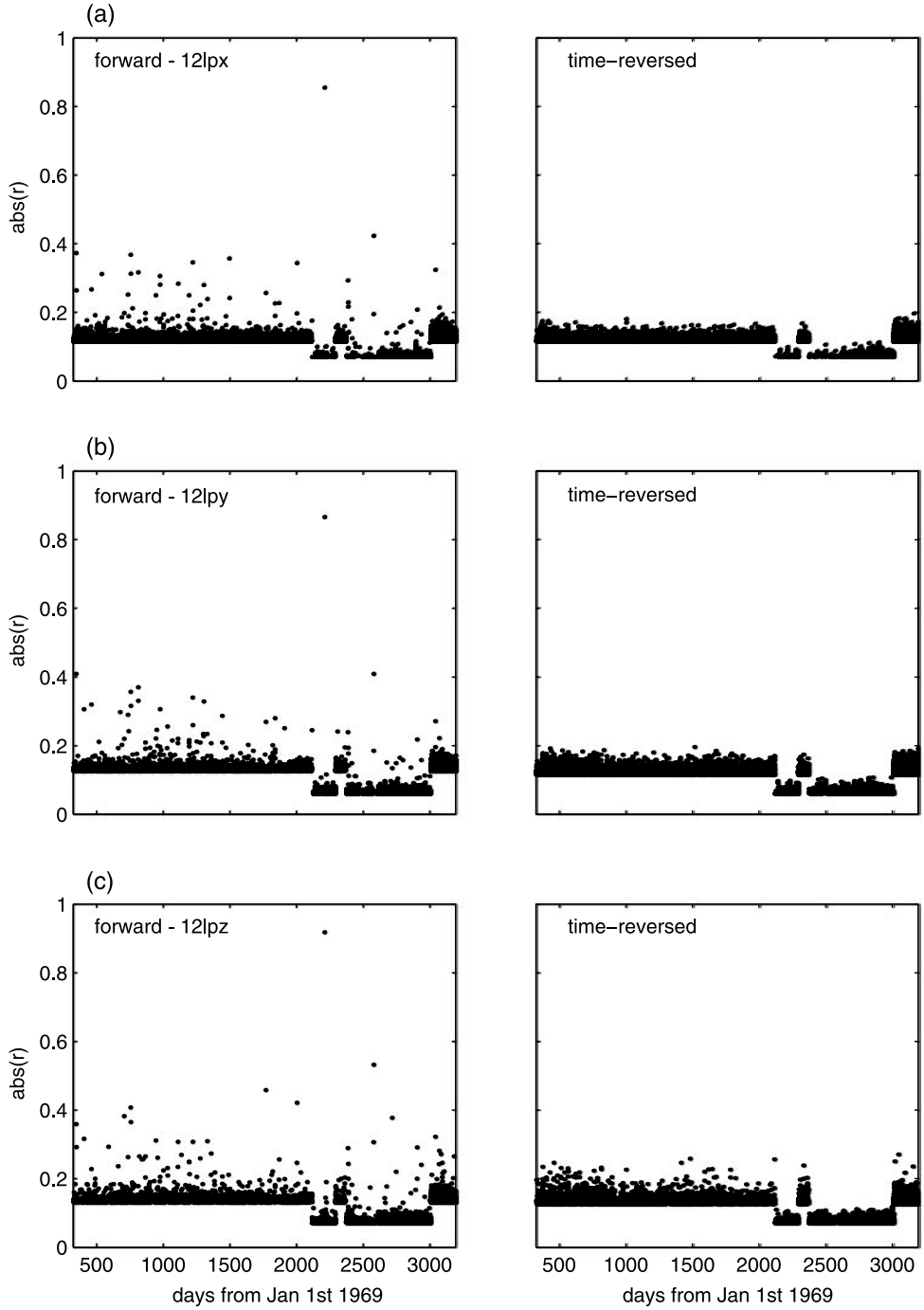

Figure 13. (a) Absolute correlation coefficient versus time for A1 lpx continuous cross correlations on station 12. The discontinuities represent times when the station was operated in the flat mode. For both the peak and flat modes the lower coefficient limit (y axis) is set depending on the overall number of correlations returned and may differ among stations or components. (b) Results for lpy. (c) Results for lpz.

[28] Among these estimation methods, the most consistent amplitudes were obtained using the 75th percentile of the absolute deviation of the data from the median (Figure 6). We consider amplitudes consistent if they exhibit similar values on the horizontal channels, corresponding to a 1:1 relationship on x component versus y component amplitude plots. Amplitude consistency between the long-period horizontal channels is shown for deep event cluster A1 in Figure 7. We have found that amplitude characteristics vary depending on the mode in which the instruments were operated. As a result, the flat and peaked modes are shown separately for stations 12, 15, and 16 (station 14 was not operated in the flat mode). Events recorded during the flat mode exhibit a clear 1:1 relationship between x and y amplitudes. In contrast, x and y component amplitude estimates for events recorded during the peak mode are less

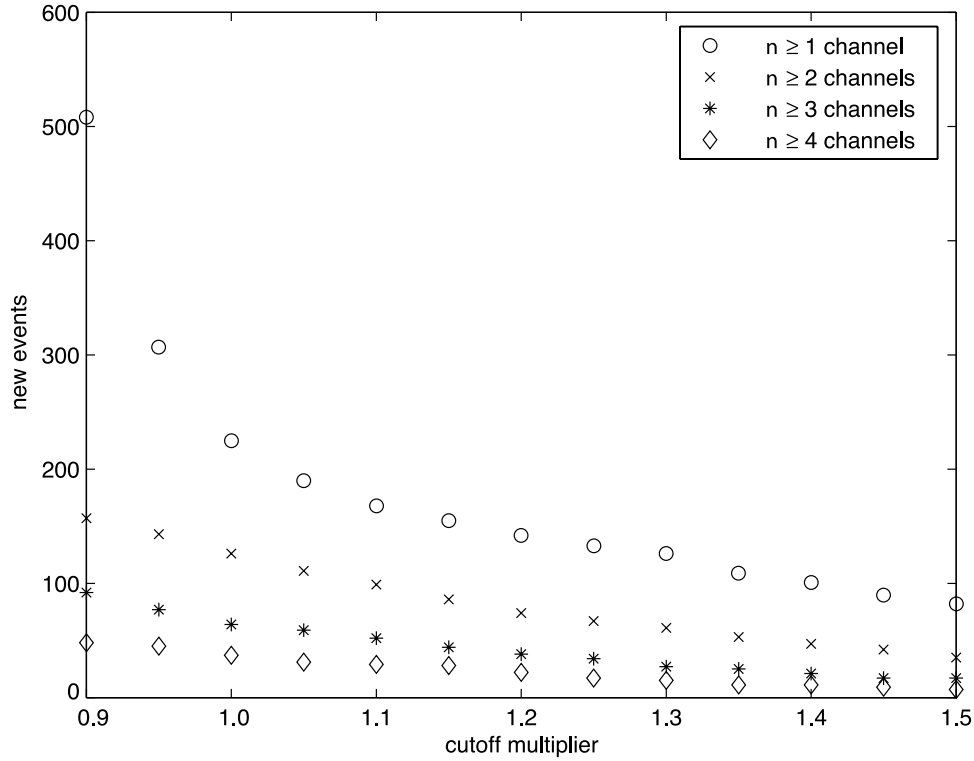

Figure 14. Number of new events versus cutoff multiplier for varying numbers of channels.

consistent. This is probably due to the fact that flat mode events tend to have better signal to noise than peak mode events. This is manifest in our grade results, which show that 23% of graded flat mode events received an A grade, while only 6% of peak mode event did so. Consequently, in further analyses we treat flat mode and peak mode recordings separately. Overall, stations 12 and 16 show the most consistent amplitudes on the horizontal channels.

3.2.2. Robust Identification of A1 Events

[29] Owing to variations in deep event classification methods and the low signal-to-noise ratio of many records, waveforms from one deep event source may be similar to those from other sources. To more accurately identify deep event group members, every event from a previously classified group is cross correlated with every other event in that group. This quantifies the level of association among members of a deep event group, identifying the best matched events. Before cross correlation, the data are filtered and despiked. A 20-min window is used in each calculation; the beginning of the window is aligned with the catalog event start time. The time shifts and relative amplitudes of the traces are recorded for the peak positive and negative correlations of two given traces. The largest absolute value of the correlation coefficient determines the event polarity. For each event pair, correlations for the three long-period channels at each station are performed separately.

[30] Histograms of correlation coefficient values for calculations performed among all A1 deep events are shown in Figure 8. Note the malfunction of the lpz component at station 14, reflected in the overall low correlation of its traces. The few high correlations (0.9 to 1.0) for 14 lpz are artifacts generated by correlations between two "flat line" traces on that channel. Another station characteristic is the low number of events with absolute values of correlation coefficient higher than 0.2 on any of the channels on station 15. This could possibly be a result of the overall low amplitude of events recorded on that station (Figure 7). Whether this reflects instrument or site characteristics is unknown, although it has been suggested that station 15 is situated in such a manner that waveforms from the A1 source vary with tidally induced changes in slip behavior (Y. Nakamura, personal communication, 2005). The overall number of correlations decreases from station 12 to 16 since stations deployed earlier recorded more events. Application of the despiking algorithm to the data before performing the cross correlations produces overall larger correlation coefficient values and improved estimates of differential times and amplitudes.

[31] "Good" correlations are identified by examining the agreement in time shifts (the time offset required to align a pair of traces for maximum cross correlation) for each event pair as a function of cross-correlation coefficient (Figure 9). Above an absolute correlation coefficient of $\sim$0.2, the median standard deviation in time shifts is less than 0.1 s, which is smaller than the data sampling interval and reflects accurate timing. Below this value, the variability in time shifts increases dramatically.

3.2.3. Stacking A1 Events

[32] We generate deep event group stacks from event pairs meeting an absolute correlation coefficient cutoff of 0.2 or higher. The traces were despiked and appropriately time shifted, and negative polarity events were flipped before stacking. We make separate stacks for both the flat and peaked station modes, and normalize the stacks by the number of contributing traces. Our cross-correlation selec-

Table 2. Newly Identified A1 Events

Year	Day[a]	Hour:Minute
1969	346	08:20
1969	348	02:30
1970	40	08:21
1970	95	23:47
1970	324	15:48
1970	342	00:48
1971	4	16:51
1971	10	08:39
1971	24	22:07
1971	25	22:48
1971	81	17:33
1971	90	08:28
1971	108	07:09
1971	134	20:56
1971	135	08:18
1971	214	12:44
1971	219	14:49
1971	220	10:40
1971	227	05:11
1971	244	06:15
1971	245	11:11
1971	246	22:57
1971	301	03:23
1971	308	18:15
1971	337	15:56
1972	13	21:37
1972	15	04:30
1972	41	00:10
1972	70	14:18
1972	80	09:24
1972	97	11:43
1972	99	03:29
1972	124	22:21
1972	126	21:36
1972	156	00:45
1972	181	13:34
1972	205	17:14
1972	209	00:13
1972	209	01:08
1972	233	08:29
1972	234	07:00
1972	234	16:56
1972	235	17:47
1972	264	08:03
1972	264	22:40
1973	10	00:22
1973	34	13:10
1973	36	16:12
1973	50	13:09
1973	155	06:48
1973	172	10:46
1973	175	01:43
1973	183	08:38
1973	187	12:42
1973	202	18:34
1973	309	05:03
1973	336	22:36
1973	337	10:59
1973	338	01:32
1973	338	10:52
1973	339	11:44
1973	350	06:02
1973	351	08:51
1974	10	16:13
1974	12	06:29
1974	41	02:18
1974	41	17:09
1974	42	05:40
1974	42	16:35
1974	70	17:25
1974	83	03:32
1974	97	21:18
1974	98	14:31
1974	110	00:32
1974	110	21:28
1974	128	19:58
1974	176	15:07
1974	205	10:16
1974	206	07:56
1974	346	02:06
1975	6	13:41
1975	22	02:06
1975	30	23:08
1975	32	11:04
1975	116	08:15
1975	194	07:07
1975	196	00:17
1975	197	01:11
1975	198	02:03
1975	198	15:17
1975	222	14:43
1975	225	21:22
1975	246	10:47
1975	252	09:35
1975	281	04:21
1975	360	00:32
1976	22	01:04
1976	23	11:14
1976	103	13:49
1976	119	12:44
1976	160	19:18
1976	190	07:08
1976	217	17:28
1976	240	15:34
1976	300	19:36
1976	347	20:07
1976	349	02:27
1977	13	02:12
1977	38	18:26
1977	77	07:01
1977	89	02:47
1977	91	22:48
1977	103	19:41
1977	119	16:01
1977	131	13:23
1977	146	03:45
1977	146	23:27
1977	148	12:23
1977	161	17:01
1977	173	07:38
1977	183	21:07
1977	258	17:10
1977	258	19:13

[a]All days are listed as Julian days.

tion criterion results in the retention of between 17% and 71% of the cataloged A1 events for the horizontal channel stacks and up to 39% of the cataloged events for vertical channel stacks (Table 1). Despiking before stacking allows for greatly improved signal to noise, as shown in Figure 10. Stacks for deep event group A1 on all long-period components are shown in Figure 11 for the peak mode and

Table 3. New A1 Events Detected per Channel

	Channel		
Station	lpx	lpy	lpz
12	82	82	67
14	60	82	4
15	12	23	6
16	61	65	28

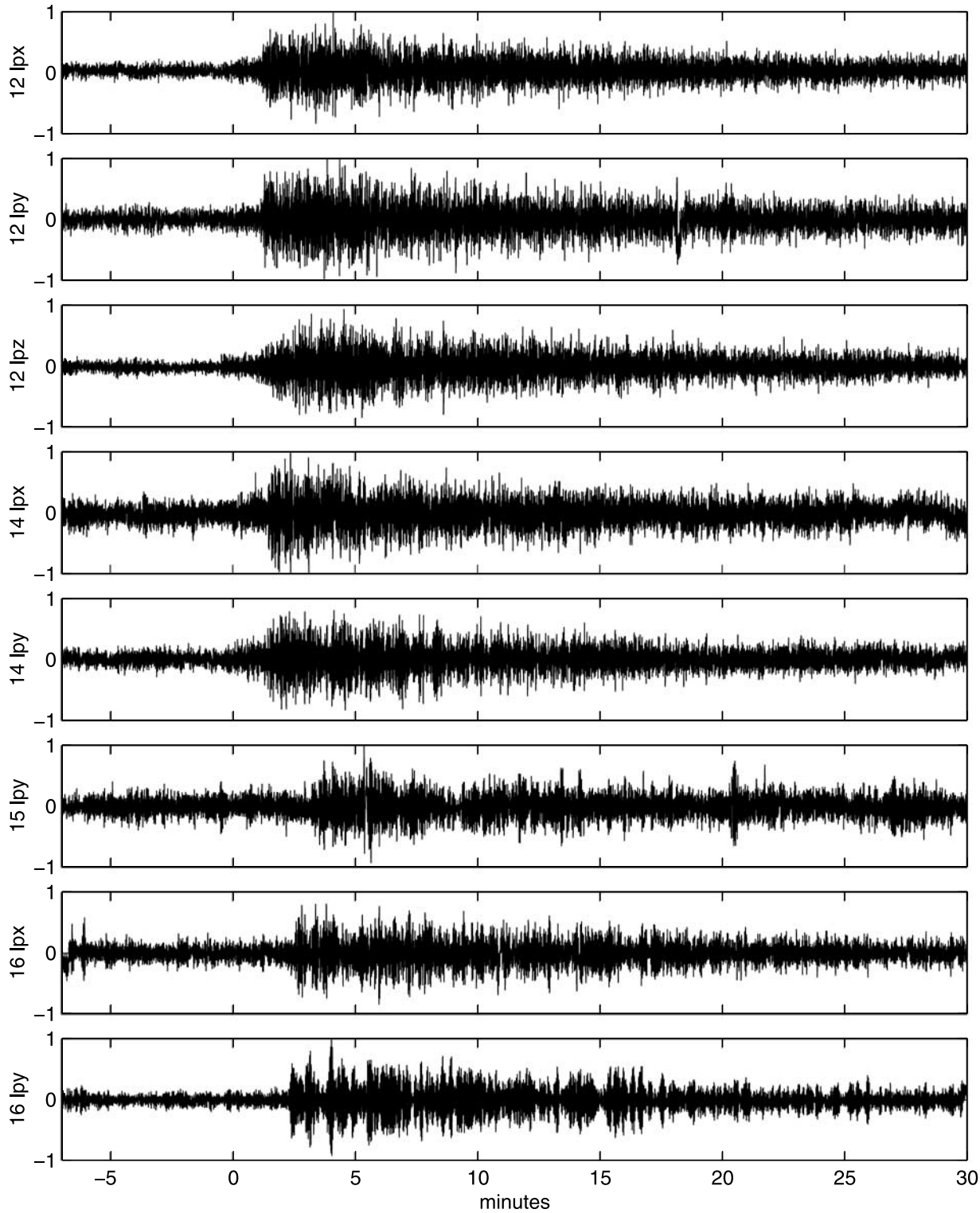

Figure 15. New event stacks for deep event group A1. Shown are stacks for station 12, lpx, lpy, and lpz; station 14, lpx and lpy; station 15, lpy; and station 16, lpx and lpy. Not shown are the channels where the number of events was too small to produce a visible signal.

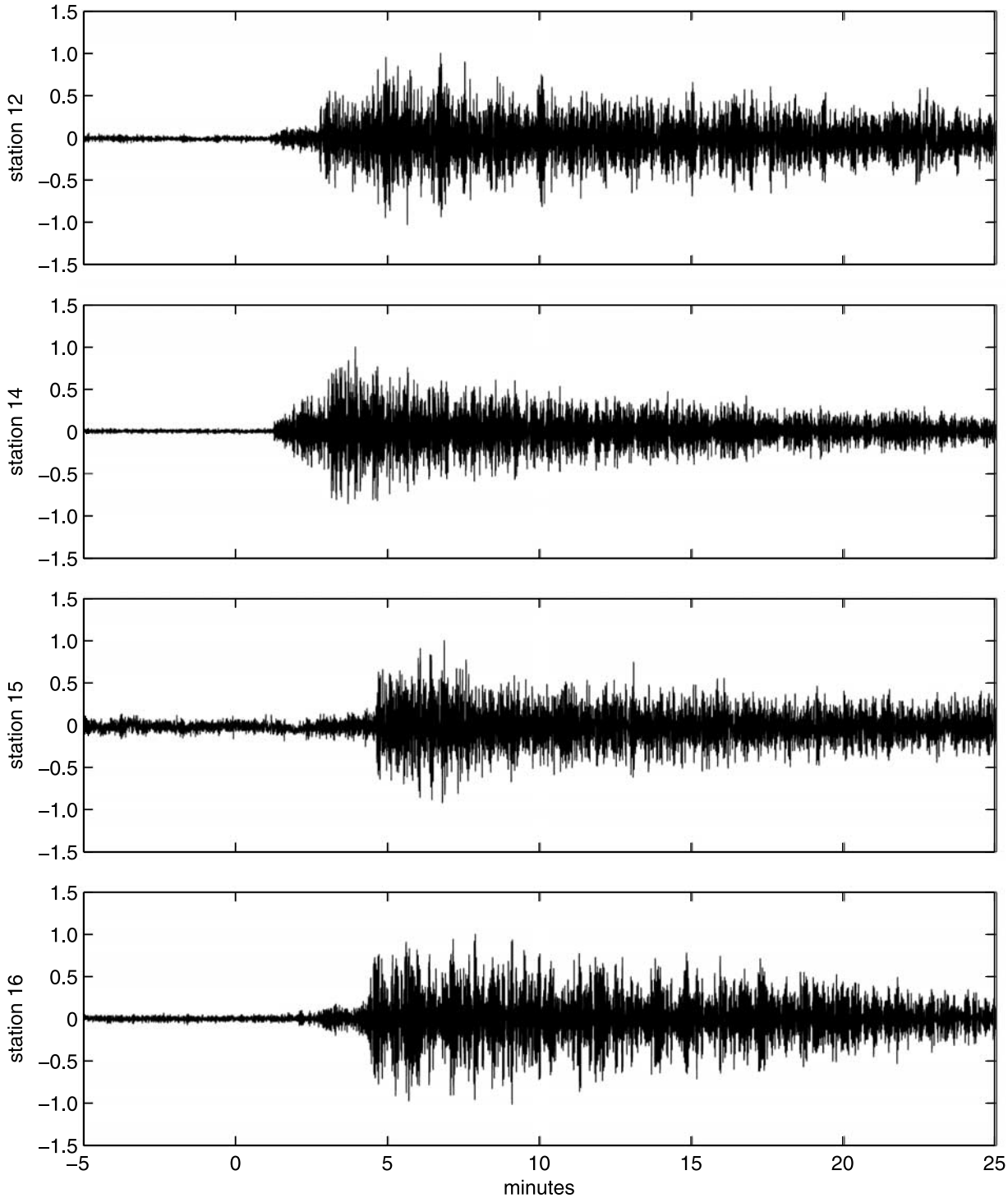

Figure 16. Optimized peak mode stacks for the lpx component on all stations.

Figure 12 for the flat mode. In general, cleaner stacks result for stations/channels with more events.

4. Search for New A1 Events in the Continuous Data

[33] To begin the search for new events in the continuous data, a target trace must be selected for cross correlation. We create and use the event data stacks described in the previous section for the deep event group A1 as identified by *Nakamura et al.* [2004]. We focus on this group because it has the largest number of cataloged events (323) of all the identified source regions. The next largest group (A8) has 224 events. In addition to being numerous, A1 events are also generally well characterized (perhaps because of the proximity of the A1 epicenter to the instruments), presenting a good starting point for the search for new events. However, our methods can be extended to other deep event groups: the main limitation is the computation time required for the continuous cross correlations.

Table 4. Number of A1 Events in Optimized Stacks

Station	Channel	Number of A1 Events
12	lpx	154
	lpy	166
	lpz	138
14	lpx	130
	lpy	191
	lpz	-
15	lpx	48
	lpy	76
	lpz	65
16	lpx	131
	lpy	46
	lpz	94

[34] We compute cross correlations of the A1 stacks with the continuous data on a station by station, component by component basis using a 30-min window of the target stack. (Peak and flat mode times are treated separately.) While the relatively long window length creates an overall reduction in correlation coefficient values, it also reduces the number of false returns. Results for the long-period components of station 12 are shown in Figures 13a–13c. The left column shows the time of occurrence of each peak in the cross-correlation function. For clarity, points representing previously cataloged events are not shown; the remaining points represent possible new events.

[35] Because the signal-to-noise ratio for events is often close to unity, absolute values of the cross-correlation coefficient (r) are typically low (see Figure 13), and it is important to establish criteria for distinguishing a potential new event from noise. We minimize incorrect detection of events in two ways. First, we observed that true cross-correlation peaks between the target trace and the continuous data often are accompanied by adjacent peaks with absolute values almost as high as that of the true peak, but located at time shifts approximated by the dominant period of the seismogram. We suppress these by not accepting peaks within $\sim$1.2 min of a peak with a higher absolute value in r (to account for polarity flips). Second, we estimate the maximum cross-correlation coefficients characteristic of noise in the data by performing cross correlations in which we time reverse the target trace. This gives a target trace with the same amplitude and frequency content as the real trace but with physically meaningless phase behavior. Cross-correlation peaks resulting from time-reversed targets provide a measure of correlated noise in the data set. Results from the time-reversed correlations performed on the long-period channels of station 12 are shown in Figures 13a–13c (right column).

[36] To ensure that our correlation method is successfully detecting new A1 events, we first check that a significant percentage of known A1 events (the points removed from the left-column plots of Figures 13a–13c) are identified. Because a subset of these events comprise the target stack, they tend to correlate highly. For the lpx, lpy, and lpz components on station 12, we successfully identify 80%, 90%, and 77% of cataloged A1 events during the continuous cross correlations, in good agreement with the percentage of events used in generating the target stacks for these channels (Table 1).

[37] To calculate the number of remaining points representing new events, we select a cross-correlation cutoff that discriminates between noise and events. In Figures 13a–13c (left), points falling above this cutoff represent new events and points falling below represent noise. This cutoff is set using a multiple of the absolute maximum correlation coefficient returned by the time-reversed correlations. We also can choose whether we require a new "event" to appear on more than one channel or station. Figure 14 shows the number of new events returned as a function of the cutoff multiplier for four different channel/station constraints.

[38] Using a cutoff multiplier of one (i.e., a threshold cross-correlation coefficient equal to the maximum value returned by the time-reversed correlations) and a channel/station constraint of two, we identify 123 new A1 events (Table 2). This is a conservative estimate; by relaxing the cutoffs we could obtain additional events at the cost of likely including some false correlations. We note that our requirements are more stringent than those originally employed in the identification of lunar events: events listed in the existing lunar catalog need only appear on a single channel on a single station. The numbers of new events observed on each station and channel are specified in Table 3. In the continuous data, most of the individual new event waveforms cannot be visually distinguished from background noise. However stacking improves the signal-to-noise ratio and the new events are visible. In Figure 15 we stack each component separately using the events listed in Table 3. Channels where the number of events was too small to produce a visible signal are not shown.

5. Discussion: Analyses of Complete A1 Cluster

[39] Our discovery of 123 new A1 events (a 38% increase) enables several avenues of further investigation. Here we report initial analyses that revise and extend previous work. Combined with the previously cataloged A1 events, we have formed a complete list of all A1 events available in the Apollo lunar seismic data. This allows us to produce improved waveform stacks for the A1 cluster using a weighted iterative stacking method. From these optimized stacks, we make seismic phase picks for comparison with picks from previous studies, and generate revised location estimates using specific velocity models. With the new catalog, we will also be better able to investigate the temporal distribution of A1 events and its implications for tidal periodicities present in A1 occurrence times.

5.1. Generation of Optimized Stacks

[40] Because A1 events in the original catalog are of variable quality, stacking these events using a simple arithmetic average of traces may not produce as clean a stack as a method that gives more weight to highly correlating traces or those having a better signal-to-noise ratio. We employ a weighted iterative stacking method to ensure events are selected and stacked to create a representative trace with high signal to noise and the clearest seismic phase arrivals. Using a single high-quality A1 event as the target trace, we perform cross correlations with all events in the new, complete catalog. This allows us to identify not

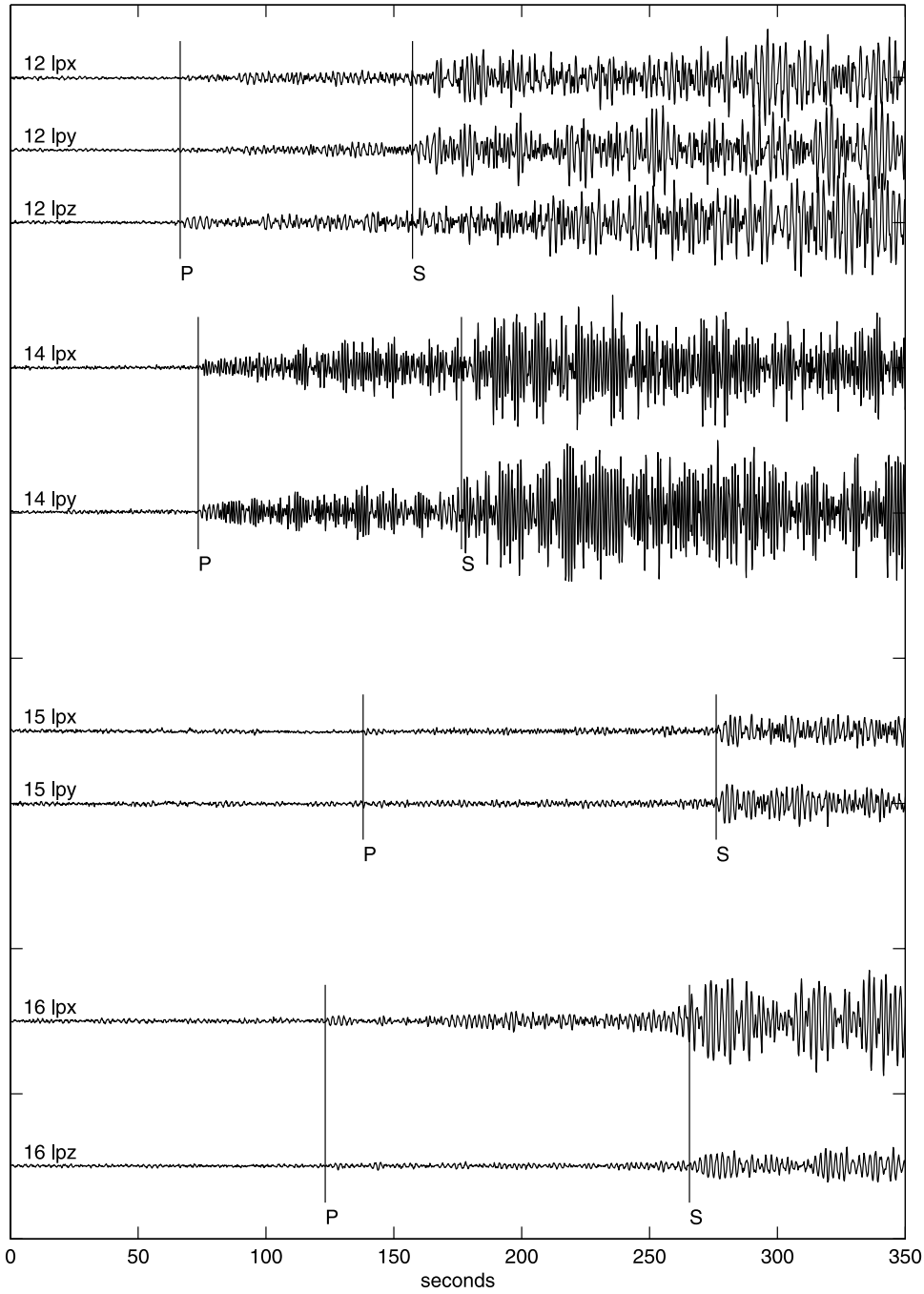

Figure 17. *P* and *S* wave arrival time picks plotted on A1 long-period event stacks for all available channels on all stations.

Table 5. A1 Picks and *S-P* Differential Times: A Comparison[a]

Station	*P*	σ_p	*S*	σ_s	*S-P* This Study	*Nakamura* [1983]	*Lognonné et al.* [2003]
12	66.4	2	157.3	10	90.9	99.7	98.1
14	73.5	3	176.5	11	103.0	103.2	105.8
15	138.0	4	276.1	9	138.1	148.1	145.8
16	123.1	4	265.7	10	142.6	137.9	138.1

[a]All picks are in seconds from reference time 1973/273 04:12; σ_p and σ_s represent uncertainty in *P* and *S* picks (seconds).

Table 6. A1 Location Estimates

Velocity Model	Norm	Latitude	Longitude	Depth, km
Lognonné et al. [2003]	L1	−11.9	−38.1	843
Lognonné et al. [2003]	L2	−13.3	−38.4	863
Nakamura [1983]	L1	−13.2	−40.8	846
Nakamura [1983]	L2	−14.3	−40.2	838
Nakamura [2005] estimate		−15.7	−36.6	867
Lognonné et al. [2003] estimate		−17.40	−38.40	917

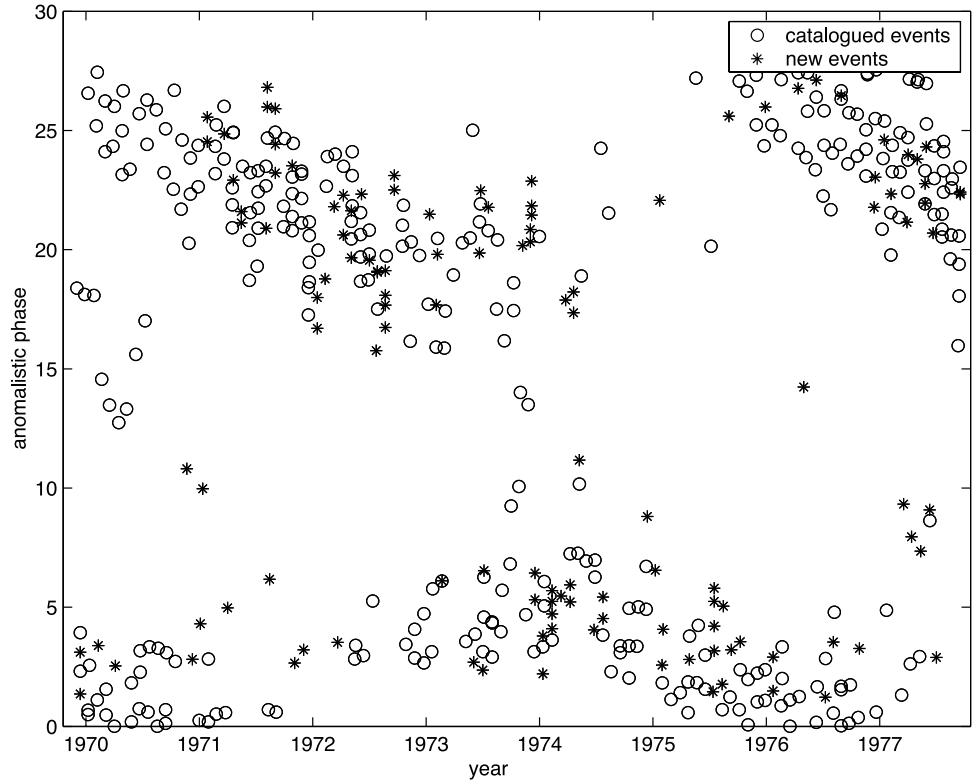

Figure 18. Anomalistic phase of new and cataloged A1 moonquake occurrences versus time. New events show phase behavior consistent with previously identified A1 moonquakes.

only known A1 events, but also A1 events that were either listed in the catalog as 'unclassified' or incorrectly classified as members of other deep clusters.

[41] Events correlating with the target at $r \geq 0.2$ are considered for stacking. Before the stack is formed, each individual trace is weighted by the squared correlation coefficient, r^2. We also attempted weighting by r, higher powers of r, and the signal-to-noise ratio, but weighting with r^2 produced a stack with the most easily discernable seismic phase arrivals. The cross-correlation procedure is then repeated, this time using the weighted stack as the target. To optimize the stack, the process is repeated until the number of events added to the stack stabilizes. We find good convergence after four iterations. Optimized peak mode stacks for the lpx component on all stations are shown in Figure 16 and the number of events in each stack is summarized in Table 4.

5.2. Travel Time Picks

[42] *P* and *S* wave arrival picks made from our optimized A1 stacks are shown in Figure 17. Our $S - P$ differential times show good agreement with comparison times from *Nakamura* [1983] and *Lognonné et al.* [2003] as summarized in Table 5. This is to be expected, as A1 is the largest and most-studied deep cluster. Future application of our method to less well-characterized clusters will be of particular interest, especially to those groups whose location has not previously been well-constrained.

5.3. Location Estimates

[43] We use the travel time picks reported in Table 5 along with two representative seismic velocity models [*Nakamura*, 1983; *Lognonné et al.*, 2003], to reestimate the A1 cluster location. Clearly, cluster location trades off with velocity structure and a more complete study would include joint forward modeling of a set of cluster locations and deep lunar velocity structure. Using an initial guess for the hypocenter location, we ray trace through a specified velocity model using a grid search algorithm to find the best fit cluster location in a least squares (L2-norm) or robust (L1-norm) sense.

[44] The L1 (L2) best fit latitude, longitude, and depth for the *Nakamura* [1983] and the *Lognonné et al.* [2003] velocity models are given in Table 6, along with a recent A1 location estimate by *Nakamura* [2005], and the estimate given in *Lognonné et al.* [2003]. Generally good agreement among location estimates is seen, as would be expected for the relatively well-characterized A1 cluster. Differences in locations reflect a combination of (1) uncertainties in travel time estimates, (2) trade-offs with velocity structure, and (3) possible spatial extent of the cluster. The largest discrepancy between our preliminary location estimates and those previously published is in the cluster depth; however, our A1 depths reported here are consistent with the recent estimate of 867 ± 29 km of *Nakamura* [2005].

5.4. Temporal Distribution

[45] A complete record of moonquake occurrence times is crucial to studying tidal triggering of moonquakes. Correlations between moonquake occurrence times and lunar tidal cycles have been noted in previous studies [*Lammlein et al.*, 1974; *Lammlein*, 1977; *Toksöz et al.*, 1977]. Using previously cataloged and our new A1 events, we tested the dependence of moonquake occurrence times on tidal varia-

tions by calculating the anomalistic phase of each event. The anomalistic month represents the time it takes the Moon to travel from one perigee to the next (~27.55 days). The anomalistic phase of our complete set of A1 moonquakes relative to a reference date is shown in Figure 18. The periodicity of A1 moonquakes is apparent, with events occurring near perigee in 1970 and gradually shifting to before perigee in 1974. New events show phase behavior consistent with previously identified A1 moonquakes, as expected. Figure 18 also illustrates how our event search fills in the temporal distribution of events.

[46] As noted by *Lammlein* [1977], A1 moonquakes are controlled not only by the anomalistic phase (most closely linked with tides), but also by the orientation of the moon's orbit with respect to the ecliptic, which is described by the nodical month (27.21 days). These two periods determine the location and orientation of the moon relative to Earth, and their sum yields a period with a "beating" that causes a phase shift every 6 years. On the anomalistic phase versus time plot in Figure 18, the shift in 1974 is due to this 6-year variation, with occurrence times gradually switching from before perigee passage to after.

[47] Robust analyses of A1 moonquake occurrence times are possible using our revised catalog. In addition, the extension of our new event search and stack optimization to all deep event clusters will create a more complete picture of the temporal and spatial distribution of lunar seismicity. Such a data set would form the basis for examining the driving mechanism of deep moonquakes.

6. Conclusions

[48] Analysis of the continuous event data has proven to be fruitful. Although previous studies did a remarkable job of identifying events by visual rather than automatic means, our comprehensive event search has shown the analysis of the continuous Apollo lunar seismic data to be worthwhile, as additional events are readily detectable using cross-correlation methods. Furthermore, modern computing capabilities have proven essential for obtaining reliable results, as lunar seismograms are of limited quality compared to terrestrial seismograms. The extensive data processing described in section 2 is essential to our results.

[49] Focusing on the A1 deep cluster has allowed us to conduct our initial investigations on a group of events with previously documented characteristics [e.g., *Lammlein*, 1977; *Lammlein et al.*, 1974; *Nakamura*, 1978; *Toksöz et al.*, 1977]. Our discovery of 123 new A1 events prompted our development of stack optimization methods, as stacking waveforms from a given deep event group provides the means for identifying seismic phases that may be difficult to discern on individual seismograms. These improved stacks have led to travel time picks and source location estimates for A1 similar to those of previous studies. For other deep event groups, which may not be as thoroughly well characterized, our approach may prove instrumental in improving our understanding of the spatial and temporal qualities of moonquake source regions.

[50] The new A1 events show occurrence patterns consistent with previously cataloged A1 events. The extension of our search to all deep event groups will provide a more complete catalog needed for further analyses of tidal variations in the deep moonquake occurrence times.

[51] **Acknowledgments.** The authors would like to thank Mary Edmunds at the IRIS DMC for help in getting the data and Yosio Nakamura for his comments, suggestions, and tireless dedication to answering questions about data formats and other issues. We thank Mark Jellinek for comments on an early draft of this manuscript and acknowledge Yosio Nakamura and Amir Khan for thorough and helpful reviews. This research was supported by NASA Planetary Geology and Geophysics grant NAG5-11563.

References

Dainty, A. M., M. N. Toksöz, and S. Stein (1976), Seismic investigation of the lunar interior, *Proc. Lunar Planet. Sci. Conf.*, *7th*, 3057–3075.

Evans, J. R. (1982), Running median filters and a general despiker, *Bull. Seismol. Soc. Am.*, *72*, 331–338.

Goins, N. R., A. M. Dainty, and M. N. Toksöz (1981), Lunar seismology: The internal structure of the Moon, *J. Geophys. Res.*, *86*, 5061–5074.

Khan, A., K. Mosegaard, and K. L. Rasmussen (2000), A new seismic velocity model for the moon from a Monte Carlo inversion of the Apollo lunar seismic data, *Geophys. Res. Lett.*, *27*, 1591–1594.

Lammlein, D. R. (1977), Lunar seismicity and tectonics, *Phys. Earth Planet. Inter.*, *14*, 224–273.

Lammlein, D. R., G. V. Latham, J. Dorman, Y. Nakamura, and M. Ewing (1974), Lunar seismicity, structure, and tectonics, *Rev. Geophys.*, *12*, 1–21.

Lognonné, P., J. Gagnepain-Beyneix, and H. Chenet (2003), A new seismic model of the Moon: Implications for structure, thermal evolution and formation of the Moon, *Earth Planet. Sci. Lett.*, *211*, 27–44.

Nakamura, Y. (1978), A_1 moonquakes: Source distribution and mechanism, *Proc. Lunar Planet. Sci. Conf.*, *9th*, 3589–3607.

Nakamura, Y. (1983), Seismic velocity structure of the lunar mantle, *J. Geophys. Res.*, *88*, 677–686.

Nakamura, Y. (2003), New identification of deep moonquakes in the Apollo lunar seismic data, *Phys. Earth Planet. Inter.*, *139*, 197–205.

Nakamura, Y. (2005), Farside deep moonquakes and deep interior of the Moon, *J. Geophys. Res.*, *110*, E01001, doi:10.1029/2004JE002332.

Nakamura, Y., F. K. Duennebier, G. V. Latham, and H. J. Dorman (1976), Structure of the lunar mantle, *J. Geophys. Res.*, *81*, 4818–4824.

Nakamura, Y., G. V. Latham, H. J. Dorman, and J. E. Harris (2004), Passive seismic experiment long-period event catalog, *Tech. Rep. 118*, rev. ed., Univ. of Tex. Inst. for Geophys., Austin.

Nakamura, Y., G. V. Latham, and H. J. Dorman (1982), Apollo lunar seismic experiment—Final summary, *Proc. Lunar Planet. Sci. Conf., 13th*, Part 1, *J. Geophys. Res.*, *87*, suppl. A117–A123.

Toksöz, M. N., et al. (1972), Velocity structure and properties of the lunar crust, *Moon*, *4*, 490–504.

Toksöz, M. N., A. M. Dainty, S. C. Solomon, and K. R. Anderson (1974), Structure of the moon, *Rev. Geophys.*, *12*, 539–567.

Toksöz, M. N., N. R. Goins, and C. H. Cheng (1977), Moonquakes: Mechanisms and relations to tidal stresses, *Science*, *196*, 979–981.

Zuber, M. T., D. E. Smith, F. G. Lemoine, and G. A. Neumann (1994), The shape and internal structure of the Moon from the Clementine Mission, *Science*, *266*, 1839–1843.

R. C. Bulow, C. L. Johnson, and P. M. Shearer, Cecil H. and Ida M. Green Institute of Geophysics and Planetary Physics, Scripps Institution of Oceanography, University of California, San Diego, 9500 Gilman Drive, Mail Code 0225, La Jolla, CA 92093-0225, USA. (rbulow@ucsd.edu)